JACS
JOURNAL OF THE AMERICAN CHEMICAL SOCIETY
Article
pubs.acs.org/JACS

Reversible and Cyclical Transformations between Solid and Hollow Nanostructures in Confined Reactions of Manganese Oxide and Silica within Nanosized Spheres

Tae-Lin Ha,[†,§] Jin Goo Kim,[‡,§] Soo Min Kim,[‡] and In Su Lee*[,‡]

[†]Department of Applied Chemistry, Kyung Hee University, Gyeonggi-do 446-701, Korea
[‡]Department of Chemistry, Pohang University of Science and Technology (POSTECH), Gyeogbuk 790-784, Korea

Supporting Information

ABSTRACT: Annealing of $MnO@SiO_2$ nanospheres in a reducing gas environment resulted in the transformation of the core−shell structure into a hollow structure as a result of outward diffusion of MnO species into the thermodynamically more stable silicate phase. When the hollow silicate nanospheres were oxidized, the interior cavities were refilled with a Mn_3O_4 phase segregated from the silicate phase, and the hollow structure reverted to the initial core−shell structure. More interestingly, when catalytically active Pt nanocrystals were introduced into the manganese oxide/silica system, the Mn_3O_4 was readily reduced to the chemically reactive MnO, even at low temperature, which enabled reconversion of the solid nanospheres with a Mn_3O_4 core to hollow nanostructures during reductive annealing. Therefore, when $MnO@SiO_2$/Pt(II) nanospheres were subjected to an oxidation/reduction cycle by repeatedly switching the flowing gas between air and hydrogen, the nanospheres underwent a reversible change between solid and hollow structures, depending on the gas environment. The solid-to-hollow-to-solid transformation was successfully cycled many times simply by repeatedly switching the flowing gas during annealing.

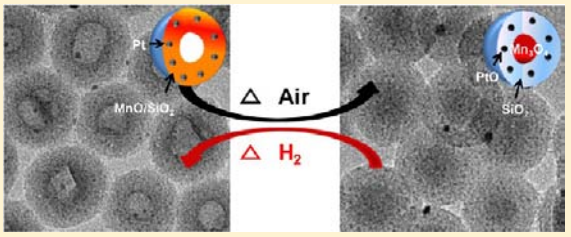

1. INTRODUCTION

Although there have been significant advances in synthetic techniques in the past two decades, enabling us to produce a variety of nanocrystals, control of their transformations between different crystalline phases and morphologies and the consequent changes in their properties still remain a significant challenge. Most of the currently available synthetic methods for the production of nanocrystals use a bottom-up process, which involves the reduction of metal precursors or the decomposition of metal complexes in a solution containing organic stabilizers.[1] Recently, the concept of "nanocrystal conversion chemistry", which involves the chemical transformation of preformed nanocrystals into new nanostructures, has emerged as an alternative approach.[2] This approach gives access to more complex materials that cannot be obtained using traditional methods.[3] In particular, the effectiveness of this strategy has been successfully proved by the production of hollow nanocrystals,[4] which have attractive properties for emerging applications, including nanoreactor,[5] drug-delivery vehicles,[6] contrast agents for molecular imaging,[7] and energy materials.[8] Most of the syntheses reported so far use the morphological transition of the precursor nanocrystals, which irreversibly proceeds from solid to hollow structures during the phase transition, using galvanic replacement,[9] diffusion-mediated chacogenization and phosphidation,[10] or ion-exchange reactions.[11] However, to date, it is still rare to find the report that deals with the reversible interchange between solid and hollow nanostructures in either solid or suspension state.[12,13]

In this context, our research have been focused on employing the solid-state conversion of nanocrystals to develop a novel fabrication method of a wide range of nanocrystalline materials based on an understanding of the solid-state reactions taking place at nanoscale.[14] In our early study on the solid-state reaction of manganese oxide nanocrystals confined within nanosized silica spheres, we had observed the thermal transformation of the core−shell type nanosphere, which is composed of a Mn_3O_4 core and a silica shell incorporating Pd/PdO nanocrystals, into hollow silicate nanostructure during the annealing process.[14a] In our continued effort to further understand the inner-cavity evolution mechanism, it was realized that the hollowing of the manganese oxide core is caused by phase transition of separate MnO and SiO_2 into a thermodynamically stable silicate phase. It was also discovered that the hollow silicate nanospheres revert to the initial core−shell structure when subjected to air oxidation, by filling of the interior cavities with a Mn_3O_4 phase segregated from the silicate phase. More interestingly, the additional incorporation of catalytically active Pt nanocrystals allows the low-temperature reduction of the Mn_3O_4 phase of the solid core into the silicate shell and thus enables reversible and cyclical trans-

Received: September 14, 2012
Published: November 8, 2012

   dx.doi.org/10.1021/ja309142j | J. Am. Chem. Soc. 2013, 135, 1378−1385

formations from solid to hollow and back to solid nanostructures during oxidation and reduction cycles (Scheme 1). In this paper, we report our findings on the reversible

Scheme 1. Reversible Transformation between Solid and Hollow Nanostructures

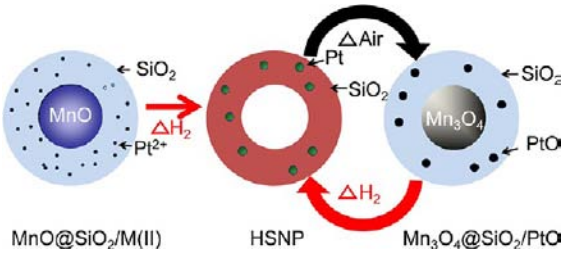

conversion between solid and hollow nanostructures, which occurs through the dimensionally confined diffusive reaction of manganese oxide and silica within nanosized spheres. We also show that the reversible transformation from solid to hollow and back to solid nanostructures can be cycled many times simply by repeatedly switching the gas environment during the annealing process. This is one of very few examples on reversible interchange between solid and hollow nanostructures. This process can enable the reversible switching of the contrasting properties of solid and hollow nanostructures.

2. EXPERIMENTAL SECTION

General Consideration. Any reagent including $MnCl_2{\cdot}4H_2O$ (Kanto), sodium oleate (TCI), 1-octadecene (Aldrich), Igepal CO-520 (Aldrich), tetraethyl orthosilicate (Acros), NH_4OH (Samchun chem.), $Ni(NO_3)_2{\cdot}xH_2O$ (Strem), $Na_2PtCl_4{\cdot}xH_2O$ (Strem), and $Na_2PdCl_4{\cdot}xH_2O$ (Strem) was used as purchased without any purification. Analyses of transmission electron microscopy (TEM) were conducted with JEOL JEM-2100F. Scanning tunneling microscopy (SEM) was carried out with XL30S FEG (Philips, The Netherlands). X-ray diffraction patterns were obtained by using X-ray diffractometer (18 kW) (Mac Science, Japan).

Preparation of MnO Nanoparticles. MnO nanoparticles were prepared by the method described previously with some modifications.[15] In a typical procedure, 12.4 g of the manganese-oleate complex (20 mmol), prepared by the reaction of $MnCl_2{\cdot}4H_2O$ and sodium oleate in a mixture of ethanol, water, and *n*-hexane, was dissolved in 100 g of 1-octadecene. The mixture solution was degassed at 70 °C for 1 h under a vacuum and then heated to 300 °C with vigorous stirring for 1 h. After cooling to room temperature, 20 mL of hexane was added to improve the dispersibility of the nanoparticles, followed by adding 80 mL of acetone to precipitate the nanoparticles. The waxy precipitate was retrieved by the centrifugation. The above purification procedure was repeated to remove excess surfactant and solvent. The purified MnO nanoparticles were dispersed in cyclohexane.

Preparation of $MnO@SiO_2$ and $MnO@SiO_2$/M(II) (M = Pt, Pd, and Ni). The $MnO@SiO_2$ nanospheres were made by modification of previously reported reverse microemulsion technique.[16]

Igepal CO-520 (1.2 mL) was dispersed in a round-bottom flask containing cyclohexane (22 mL) by sonication. Next, 10 mg of MnO nanoparticles (8.1 Mn-mg) dispersed in cyclohexane was added to the reaction solution. The resulting mixture was vortexed until the mixture became transparent. An aqueous ammonium hydroxide solution (30%, 0.13 mL) was successfully added to the reaction mixture to form a transparent suspension. Lastly, tetraethyl orthosilicate (0.4 mL, TEOS) was added, and stirred for 15 h. The resulting $MnO@SiO_2$ nanosphere in which a MnO core is surrounded by a SiO_2 shell, was collected by the centrifugation. The collected $MnO@SiO_2$ nanospheres were purified by repeating the redispersion in EtOH and water and then by centrifugation (5.7 Mn-mg, 70% of isolated yield based on Mn contents determined by the inductively coupled plasma atomic emission spectrometry, ICP-AES). The organic content of the $MnO@SiO_2$, determined by the thermogravimetry analysis (TGA), was 14%.

The $MnO@SiO_2$/M(II) (M = Pt, Pd, and Ni) nanospheres, which contain MnO nanocores and M^{2+} complexes distributed over the silica shell, were prepared through the same procedure with that applied for $MnO@SiO_2$, except for the use of 0.8 mL of Igepal CO-520 and the addition of aqueous Na_2PtCl_4, Na_2PdCl_4, and $Ni(NO_3)_2$ solutions (4.7 mg/mL, 0.2 mL), respectively, just before the addition of ammonium hydroxide solution. Isolated yields of $MnO@SiO_2$/Pt(II), 75% (14% of organic content); $MnO@SiO_2$/Pd(II), 89% (17% of organic content); $MnO@SiO_2$/Ni(II), 80% (15% of organic content).

Oxidative and Reductive Annealing of $MnO@SiO_2$/M(II) (M = none, Pt, Pd, and Ni). In a typical annealing procedure, the powders were placed in a tube-type furnace, respectively, heated up with 5 °C/min, and annealed at various temperatures in a range 500−800 °C. For the reductive and oxidative treatment, the annealing procedure was performed under air environment and under a flow of Ar + 4% H_2, respectively. M-HSNP-500, -600, -700, and -800 (M = none, Pt, and Pd) and Ni@HSNP-500, -600, -700, and -800 were prepared by reductively annealing $MnO@SiO_2$/M(II) (M = none, Pt, Pd, and Ni) at various temperature for 2 h. $Mn_3O_4@SiO_2$, $Mn_3O_4@SiO_2$/M(II)O (M = Pt and Pd), and $NiMn_2O_4@SiO_2$ were produced by annealing M-HSNP-500 (M = none, Pt, Pd,) and Ni@HSNP-500 in air at 500 °C for 2 h, respectively. The experiment for investigating possibility of the cyclic solid-to-hollow-to-solid transformations were performed with $MnO@SiO_2$/Pt(II) by repeatedly applying the reductive and oxidative annealing for 5 h, respectively. Isolated yields of HSNP-500, 83%; -600, 94%; -700, 84%; -800, 83% ; Pt-HSNP-500, 84%; -600, 94%; -700, 89%; -800, 80% ; Pd-HSNP-500, 84%; -600, 91%; -700, 83%; -800, 94%; Ni@HSNP-500, 80%; -600, 94%; -700, 84%; -800, 88%; $Mn_3O_4@SiO_2$, 94%; $Mn_3O_4@SiO_2$/PtO, 87%; $Mn_3O_4@SiO_2$/PdO, 96%; $NiMn_2O_4@SiO_2$, 92%.

Control Experiment with Ni^{2+} Complexes Incorporating Silica Nanospheres. Silica nanospheres containing Ni^{2+} complexes were synthesized in the absence of MnO nanoparticles, for the control purpose, and annealed at high temperature. In the preparation procedure, an aqueous solution of $Ni(NO_3)_2$ (32 mg, 0.35 mL) was added to a cyclohexane solution (228 mL) containing 5.0 mL of Igepal CO-520, which followed by the addition of an ammonium hydroxide solution (0.13 mL). TEOS (1.5 mL) was then added and stirred for 15 h. The silica nanospheres containing Ni^{2+} complexes were collected by centrifugation and washed several times with EtOH and H_2O. The annealing of the silica nanospheres containing Ni^{2+} complexes was conducted under a flow of Ar + 4% H_2 at 600 °C for 2 h (heating rate 5 °C/min).

TEM Sample Preparation. For the TEM sample preparation, a small amount of the annealed powder was added to a 0.5 mL of distilled water (in an Eppendorf safe-lock microcentrifuge tube with 1.5 mL capacity) and then sonicated for a few minutes to disperse the nanoparticles into a suspension. A drop of the resulting suspension was then instilled on the standard TEM grid (carbon coated Cu grid with 3.05 mm of diameter) and dried in air.

3. RESULTS AND DISCUSSION

3.1. Solid-to-Hollow Transformation of $MnO@SiO_2$. Core−shell nanospheres, $MnO@SiO_2$, consisting of 15 (±3) nm MnO cores and SiO_2 shells of average thickness 10 (±1) nm, were synthesized by encapsulating oleic-acid-stabilized MnO nanoparticles with silica shells using a modified reverse-microemulsion technique.[16] When the $MnO@SiO_2$ nanospheres were treated under a flow of Ar + 4% H_2, which protects the MnO core against oxidation, hollowing of the MnO core was observed to be brought about by annealing at temperatures above 500 °C. The transmission electron microscopy (TEM) images of the samples obtained after reductive annealing at 500 °C for different periods showed that void spaces began to appear upon reaching 500 °C, and further

dx.doi.org/10.1021/ja309142j | J. Am. Chem. Soc. 2013, 135, 1378−1385

developed as annealing proceeded (Figure 1). The TEM image after annealing for 5 h showed the conversion of 80% of the

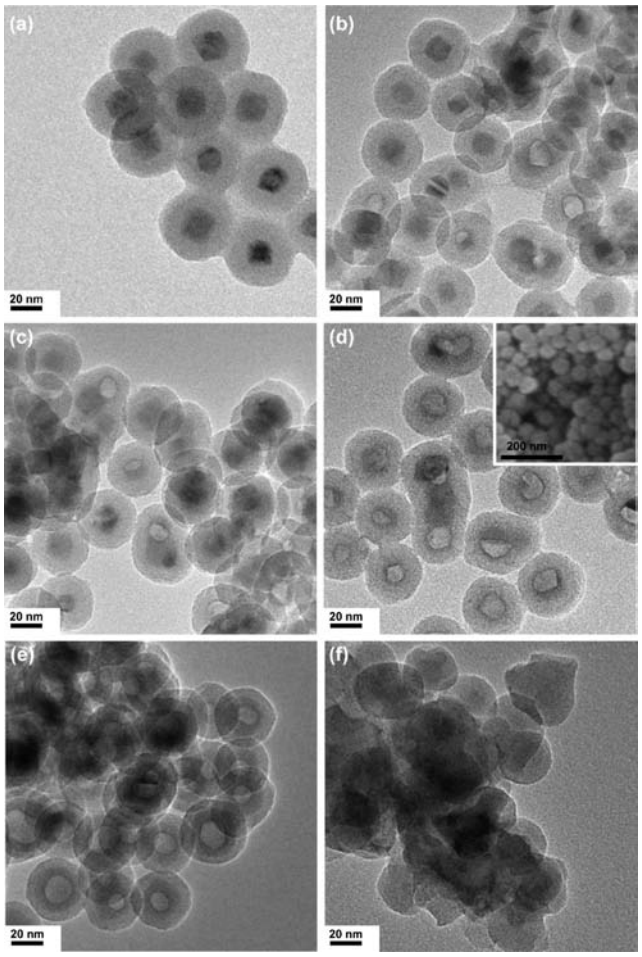

Figure 1. TEM images of the $MnO@SiO_2$ nanospheres (a) before and after the annealing under the reductive environment at 500 °C for (b) 0 h, (c) 2 h, and (d) 5 h, (e) at 600 °C for 2 h, and (f) at 700 °C for 5 h. Inset of (d) SEM image of the HSNP-500.

nanospheres initially having solid cores into structures with hollow interiors of 12 (±4) nm average diameter. Scanning electron microscopy (SEM) analysis showed that the exterior morphology of the silica sphere was preserved during the hollowing process. Annealing at 600 °C resulted in more rapid development of the hollow cavities, leading to a solid-to-hollow conversion of 92% of the nanospheres within 2 h. At higher temperatures, such as 700 and 800 °C, the hollow nanostructures collapsed and coalesced into irregularly shaped grains. X-ray diffraction (XRD) analysis showed that the reflection peaks of the MnO phase of the $MnO@SiO_2$ decreased with increasing annealing temperature from 500 to 800 °C, and the full set of reflection peaks corresponding to the Mn_2SiO_4 phase appeared after annealing at 800 °C. This indicates that the MnO and SiO_2 species, each initially separated in the core and shell areas of $MnO@SiO_2$, were mixed together, while preserving their oxidation states, at high enough temperatures to allow atomic migration, and developed into the more stable crystalline phase Mn_2SiO_4 phase (Figure 2).[17] It has previously been noted that the formation of manganese silicate from mixtures of MnO and SiO_2 is a thermodynamically favorable process.[18] Therefore, it can be

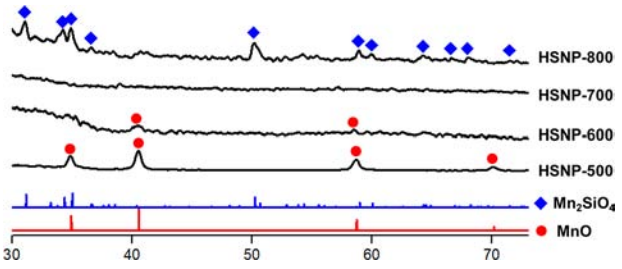

Figure 2. XRD patterns of the $MnO@SiO_2$ nanosphere before and after the annealing at various conditions.

understood that the hollowing process was driven most likely by the higher thermodynamic stability of the resulting Mn_2SiO_4 phase. Therefore, it can be understood that the hollowing process does not involve any redox reaction and is driven mainly by the higher thermodynamic stability of the resulting Mn_2SiO_4 phase. The observed hollowing phenomenon can be explained by a nanoscale Kirkendall mechanism, in which outward diffusion of fast-moving MnO species is dominant over inward transport of SiO_2.[19] The outward diffusion of Mn in the hollowing process of $MnO@SiO_2$ may be inferred from the gradual expansion of the dark TEM contrast from core to shell during development of the interior cavity.

3.2. Hollow-to-Solid Transformation of HSNPs. When the $MnO@SiO_2$ nanospheres were treated under an air atmosphere, the MnO core was oxidized to the Mn_3O_4 phase, while preserving its initial shape and size, thus generating $Mn_3O_4@SiO_2$ nanospheres with a core−shell structure. The successive annealing of $Mn_3O_4@SiO_2$ did not cause any further changes in the morphology and crystalline phases, even in a reducing-gas environment (Figure S1). This is probably because the Mn_3O_4 phase and SiO_2 are immiscible. On the basis of this, we hypothesized that the oxidation of the MnO−SiO_2 mixture phase might cause a shift in the phase equilibrium and induce further changes in the hollow morphology of HSNPs. When HSNP-500 was treated in air at 500 °C to test our hypothesis, it was found that the interior cavity became filled with a crystalline core, and as a result, the hollow structure was converted back to a solid-core structure. TEM, high-resolution TEM (HRTEM), and SEM analyses revealed that air-annealing returned the hollow nanospheres of HSNP-500 to the initial core−shell structure (Figure 3). The Mn_3O_4 crystalline phase of the core, which was identified by HRTEM and XRD analyses, indicated that the resulting nanospheres were chemically and morphologically almost identical to the $Mn_3O_4@SiO_2$ nanospheres that were obtained by annealing $MnO@SiO_2$ in air. The observed hollow-to-solid transformation can be explained by a miscible-to-immiscible phase transition of the manganese oxide−SiO_2 system; that is, oxidative annealing of HSNP-500 resulted in generation and segregation of the SiO_2-immiscible Mn_3O_4 species from the MnO−SiO_2 mixture phase into crystalline grains inside the cavity.[20] Unlike HSNP-500, HSNP-600, which is presumed to have progressed further toward the crystalline silicate phase, did not undergo morphology changes during annealing. This suggests that a metastable, amorphous, and compositionally mixed state of the intermediate MnO−SiO_2 phase is responsible for the hollow-to-solid conversion of HSNP-500.[21] The successive morphological changes from solid-core $MnO@SiO_2$ to hollow-core HSNP-500, and back to solid-core $Mn_3O_4@SiO_2$, led us to anticipate fully reversible and cyclic

dx.doi.org/10.1021/ja309142j | J. Am. Chem. Soc. 2013, 135, 1378−1385

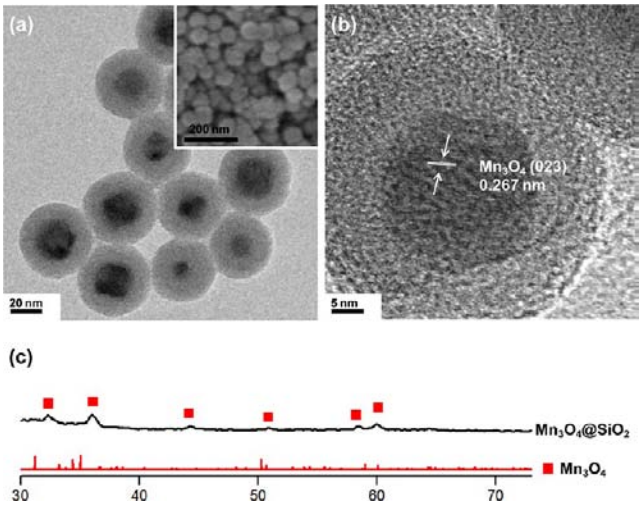

Figure 3. (a) TEM and (b) HRTEM images and (c) XRD pattern of the Mn_3O_4@SiO_2 obtained by annealing of HSNP-500 at 500 °C in air. Inset of (a) SEM image of Mn_3O_4@SiO_2.

transformations between solid and hollow interior structures. However, since the Mn_3O_4 phase is not readily reducible by annealing, the transformation cycle, which would involve conversion of Mn_3O_4@SiO_2 to HSNP-500, was not completed.

3.3. Solid-to-Hollow-to-Solid Transformation of MnO@SiO_2/Pt(II) and MnO@SiO_2/Pd(II). With a view to achieving the complete cycle of the solid-to-hollow-to-solid transformation, we introduced noble-metal nanocrystals, such as Pt, Pd, and Ni, which might catalyze the catalytic the reduction of the Mn_3O_4 phase. The incorporation of the catalytic metal species was conducted by injecting aqueous solutions containing Na_2PtCl_4, Na_2PdCl_4, and $Ni(NO_3)_2$, respectively, into the microemulsion suspension that was previously used for the synthesis of MnO@SiO_2 nanospheres. TEM images of the resulting solids showed the formation of MnO@SiO_2/M(II) (M = Pt, Pd, and Ni) nanospheres, which contained MnO cores and silica shells incorporating, Pt^{2+}, Pd^{2+}, and Ni^{2+} complexes. When MnO@SiO_2/Pt(II) nanospheres were treated under a flow of Ar + 4% H_2 at 500 °C, hollowing of the MnO cores proceeded more rapidly and more apparently than in the case of MnO@SiO_2. All the nanospheres were completely transformed to the hollow state within 2 h, resulting in the formation of homogeneous products with spherical interior cavities (Figure 4). The complete transformation of crystalline grains inside the cavities was also supported by the much diminished MnO peaks in the XRD pattern (Figure 5). The cavity evolution process for MnO@SiO_2/Pt(II) was somewhat different in detail from that for MnO@SiO_2; multiple numbers of voids emerged simultaneously in the MnO core, expanded together as annealing proceeded, and finally merged into spherical cavities. The hollow transformation was accompanied by conversion of Pt^{2+} complexes to tiny Pt nanocrystals. The resulting Pt-HSNP nanospheres therefore consisted of a hollow silicate shell with inner and outer diameters of 13 (±3) nm and 32 (±2) nm, respectively, and embedded Pt nanocrystals. Increasing the annealing temperature of MnO@SiO_2/Pt(II) to 700 °C caused the collapse of the hollow nanostructures and coalescence of the Pt nanocrystals into larger grains. The XRD analysis indicated transition of the intermediate MnO−SiO_2 phase into a crystalline silicate with XRD-detectable grain sizes, even at

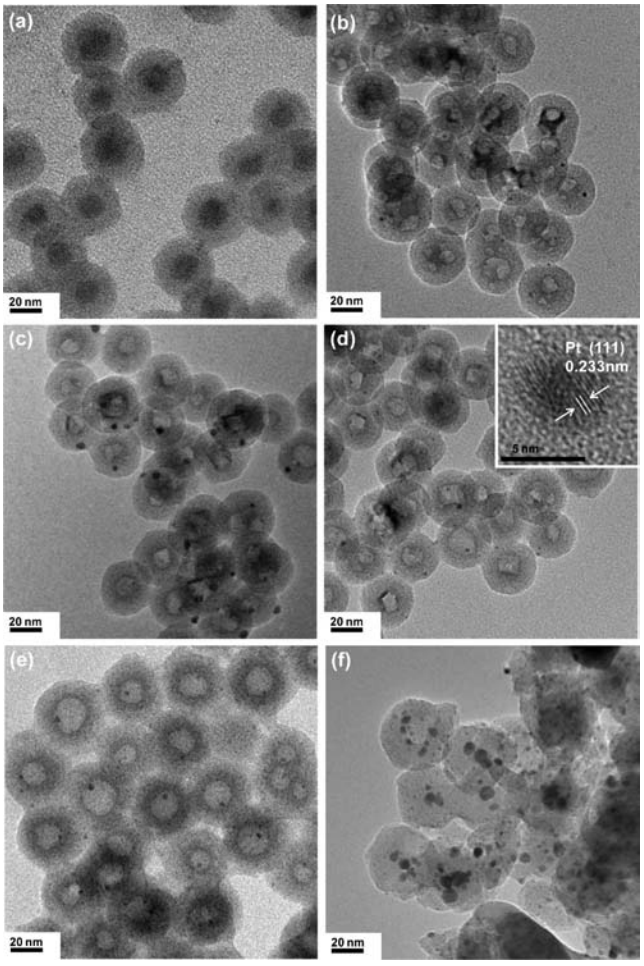

Figure 4. TEM images of the MnO@SiO_2/Pt(II) nanospheres (a) before and after the annealing under the reductive environment at 500 °C for (b) 0 h, (c) 2 h, and (d) 5 h, (e) at 600 °C for 2 h, and (f) at 700 °C for 5 h. Inset of (d) HRTEM image for showing crystalline lattice of Pt phase.

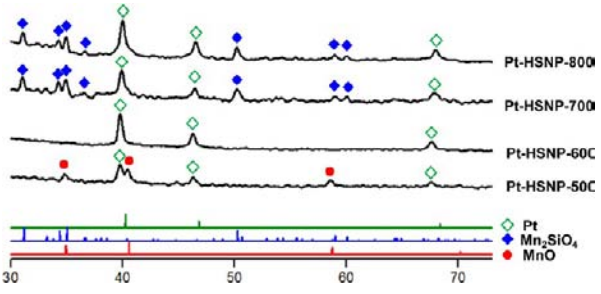

Figure 5. XRD patterns of the MnO@SiO_2/Pt(II) nanosphere before and after the annealing at various conditions.

700 °C, which is lower than the corresponding temperature for MnO@SiO_2. The enhanced transformability of the MnO@SiO_2/Pt(II) nanospheres may be attributed to the generation of catalytic Pt nanocrystals, which enable the low-temperature reduction of the passivated Mn_3O_4 layer on the core surface into the chemically labile MnO phase. The MnO@SiO_2/Pd(II) nanospheres showed similar transformation behavior to that of MnO@SiO_2/Pt(II); Pd-HSNP nanospheres with hollow interior cavities were generated by reduction at 500 and 600 °C (Figures 6 and 7). The only distinct difference between their phase transitions was the crystalline polymorph of the

dx.doi.org/10.1021/ja309142j | J. Am. Chem. Soc. 2013, 135, 1378−1385

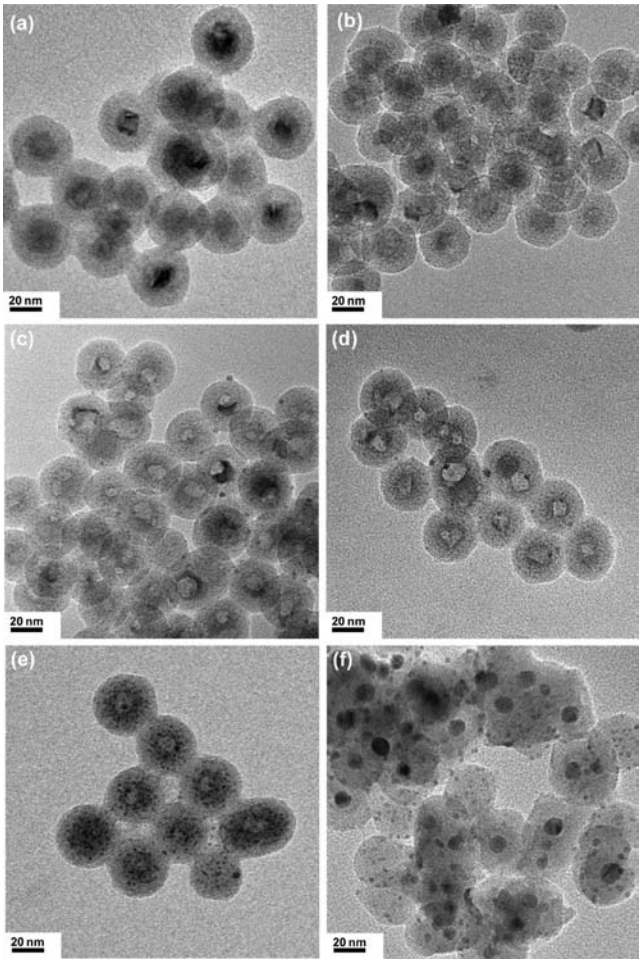

Figure 6. TEM images of the MnO@SiO_2/Pd(II) nanospheres (a) before and after the annealing under the reductive environment at 500 °C for (b) 0 h, (c) 2 h, and (d) 5 h, (e) at 600 °C for 2 h, and (f) at 700 °C for 5 h.

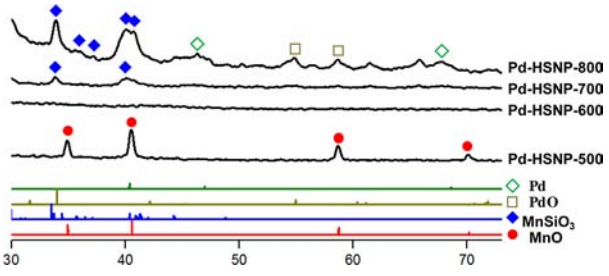

Figure 7. XRD patterns of the MnO@SiO_2/Pd(II) nanosphere before and after the annealing at various conditions.

resulting silicate; a $MnSiO_3$ phase resulted from the annealed MnO@SiO_2/Pd(II), but in the case of MnO@SiO_2/Pt(II), Mn_2SiO_4 developed as a crystalline silicate phase. Although the reaction mechanism is not fully understood, it may be inferred that the $MnSiO_3$ is favored in the equilibrium among manganese silicate species to by the embedded Pd nanoparticles.[22]

When the Pt-HSNP-500 and Pd-HSNP-500 nanospheres were oxidized by annealing in air, their interior cavities were all refilled with crystalline grains, and thus their hollow structures returned to the initial core–shell structures. The HRTEM and XRD analyses of air-annealed Pt-HSNP-500 and Pd-HSNP-500 powders at 500 °C revealed the growth of Mn_3O_4 grains, respectively, inside the cavities (Figure 8). It was also observed

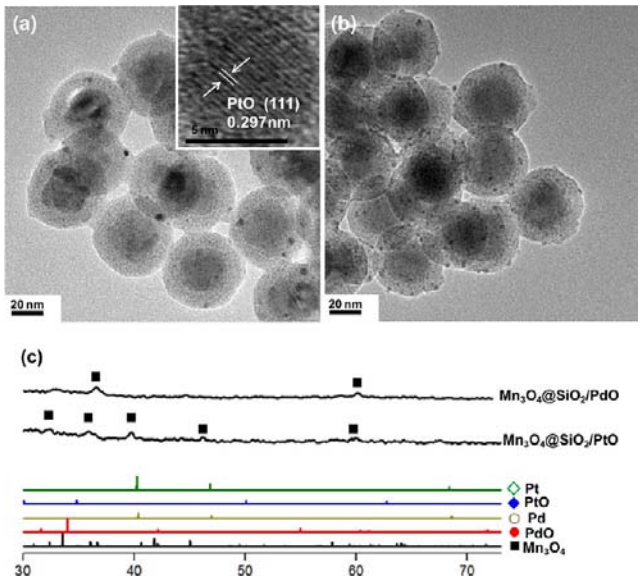

Figure 8. TEM images (a) the Mn_3O_4@SiO_2/PtO, (b) the Mn_3O_4@SiO_2/PdO, and (c) their XRD patterns. Inset of (a) HRTEM image for showing crystalline lattice of PtO phase.

that the embedded Pt and Pd nanocrystals were oxidized to PtO and PdO, respectively, which resulted in the formation of Mn_3O_4@SiO_2/PtO or Mn_3O_4@SiO_2/PdO nanospheres, each consisting of Mn_3O_4 nanocrystals in the core and multiple numbers of PtO or PdO nanocrystals embedded in the silica shell.

3.4. Reversible and Cyclical Transformations between Solid and Hollow Nanostructures. In order to verify the feasibility of fully reversible conversion between the hollow and solid nanostructures, we examined the possible reversion of the solid-core structures of Mn_3O_4@SiO_2/PtO and MnO@SiO_2/Pt to hollow structures in a reducing environment. When Mn_3O_4@SiO_2/PtO nanospheres were annealed under a flow of Ar + 4% H_2 at 500 °C, hollowing of the core and regeneration of the interior cavity occurred within 5 h. The resulting nanostructure, which consisted of a hollow shell with an inner diameter of 11 (±3) nm and an outer diameter of 32 (±2) nm, and several embedded Pt nanocrystals, was identical to that of the Pt-HSNP-500 initially prepared from MnO@SiO_2/Pt(II) (Figure S2). From the inertness of the Mn_3O_4@SiO_2 nanospheres under the same conditions, it was deduced that the conversion of the Mn_3O_4@SiO_2/PtO nanospheres to a hollow structure might be ascribed to the presence of Pt, which can catalyze the reduction reactions. In our efforts to further understand the hollow transformation mechanism, it was found that the reductive annealing of Mn_3O_4@SiO_2/PtO at 200 °C caused the reduction of Mn_3O_4 and PtO to MnO and Pt, respectively, while preserving the sizes and shapes of the nanocrystals (Figure 9a). This resulted in formation of MnO@SiO_2/Pt containing a MnO nanocore and small Pt nanocrystals distributed around the silica shell. Considering that a high temperature, above 1300 °C, is required for the reduction of the bulk Mn_3O_4 phase, the reductive transition of Mn_3O_4@SiO_2/PtO at a temperature as low as 200 °C is quite unusual.[23] When silica nanospheres containing Mn_3O_4 nanoparticles prepared without addition of a Pt^{2+} complex were annealed

dx.doi.org/10.1021/ja309142j | J. Am. Chem. Soc. 2013, 135, 1378–1385

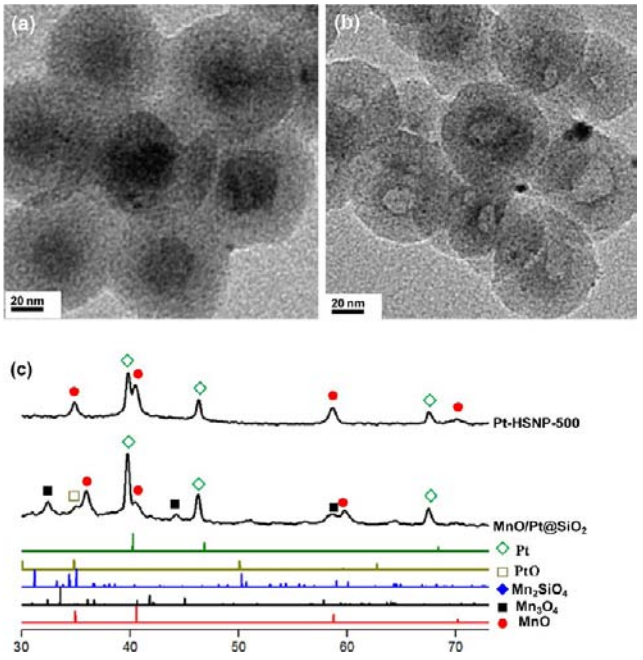

Figure 9. TEM images of (a) the $MnO@SiO_2/Pt$ and (b) the Pt-HSNP regenerated by reductively annealing the $MnO@SiO_2/Pt$ at 500 °C and (c) their XRD patterns.

in a hydrogen atmosphere as a control, the reduction of Mn_3O_4 was not observed, even at 800 °C.

The enhanced reducibility of $Mn_3O_4@SiO_2/PtO$ can be understood in terms of a Pt-catalyzed process involving the spillover of hydrogen atoms from the surfaces of prereduced Pt nanocrystals, and nanometer-distance migration of the hydrogen atoms over the silica matrix to reach and reduce Mn_3O_4.[24] It was observed that the $MnO@SiO_2/Pt$ was also converted to a hollow structure by subsequent annealing at 500 °C (Figure 9b). From these observations, the hollow transformation of $Mn_3O_4@SiO_2/PtO$ can be explained by a mechanism involving successive steps, namely generation of Pt nanocrystals from PtO, the Pt-catalyzed reduction of the Mn_3O_4 phase to the MnO phase, and outward diffusion of the reduced MnO species into the silicate phase. The reverted Pt-HSNP nanospheres were found to be reconverted to the solid-core structure of $Mn_3O_4@SiO_2/PtO$ during progressive oxidation treatments. The reductive annealing of $Mn_3O_4@SiO_2/PdO$ also resulted in transformation to hollow Pd-HSNP; this is similar to the results observed for $Mn_3O_4@SiO_2/PtO$ (Figure S3).

The observation of a series of transformations encouraged us to investigate the possibility of fully reversible and cyclic transformations between solid and hollow nanostructures. For this purpose, $MnO@SiO_2/Pt(II)$ nanospheres were subjected to an oxidation and reduction cycle by repeatedly switching the flowing gas between air and hydrogen during annealing at 500 °C. The morphology changes were monitored by sampling the annealed products between individual steps. As shown in Figure 10, the TEM images of the annealed products revealed the successive transformation of the nanospheres from solid $MnO@SiO_2/Pt(II)$ to hollow Pt-HSNP to solid $Mn_3O_4@SiO_2/PtO$, followed by a repeating transformation cycle between Pt-HSNP and $Mn_3O_4@SiO_2/PtO$. Elementary mapping analyses using energy-dispersive X-ray spectroscopy (EDX) showed localization of Mn species at the shell for the hollow Pt-HSNP nanospheres and in the core region for the solid (Figure 11).

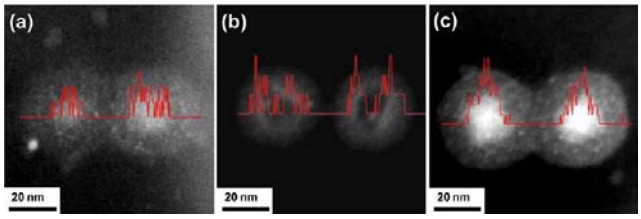

Figure 11. Dark field STEM images of (a) the $MnO@SiO_2/Pt(II)$, (b) the Pt-HSNP, and (c) the $Mn_3O_4@SiO_2/PtO$, which carry the EDX line profiles for showing the Mn distribution.

$MnO@SiO_2/Pt(II)$ nanospheres, which support reversible diffusion of the Mn species outward from the core into the shell, and from the shell to the core, during the oxidation and reduction processes, respectively. It was therefore clearly shown that the $MnO@SiO_2/Pt(II)$ nanospheres underwent reversible changes between solid and hollow structures of the oxidized Mn_3O_4 and reduced $MnO\text{-}SiO_2$ phases, respectively, as a function of the gas environment, and the solid-to-hollow-to-solid transformation was successfully cycled many times simply by repeatedly switching the flowing gas during annealing

3.5. Transformation of $MnO@SiO_2/Ni(II)$. While the $MnO@SiO_2/Ni(II)$ nanosphere were also converted into the structure with inner-cavity by the reductive annealing, its

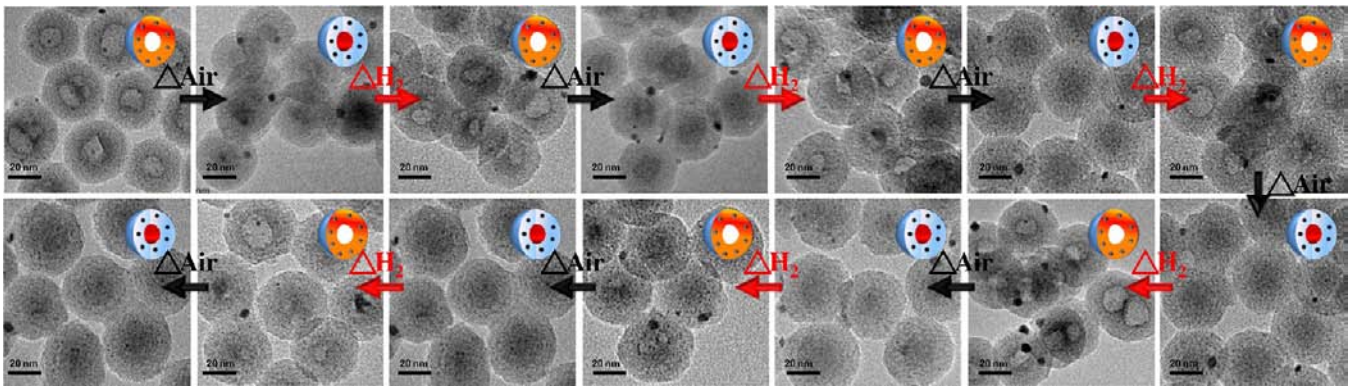

Figure 10. TEM images for showing the cyclical transformation between solid and hollow interior structure during the successive annealing at 500 °C with repeatedly switching the flowing gas between air and hydrogen .

dx.doi.org/10.1021/ja309142j | J. Am. Chem. Soc. 2013, 135, 1378−1385

hollowing process was somewhat different in detail from those for $MnO@SiO_2/Pt(II)$ and $MnO@SiO_2/Pd(II)$. Therefore, it was found that a single Ni grain was initially created at the interface between MnO and SiO_2, and then guided the formation and expansion of a void space in its vicinity, generating a rattlelike structure of Ni@HSNP which consists of a hollow silica shell with inner and outer diameters of 11 (±5) nm and 32 (±2) nm, respectively, and a single Ni nanocrystal with an average size of 6 (±1) nm captured inside the cavity (Figure 12). It may be inferred from this observation that the

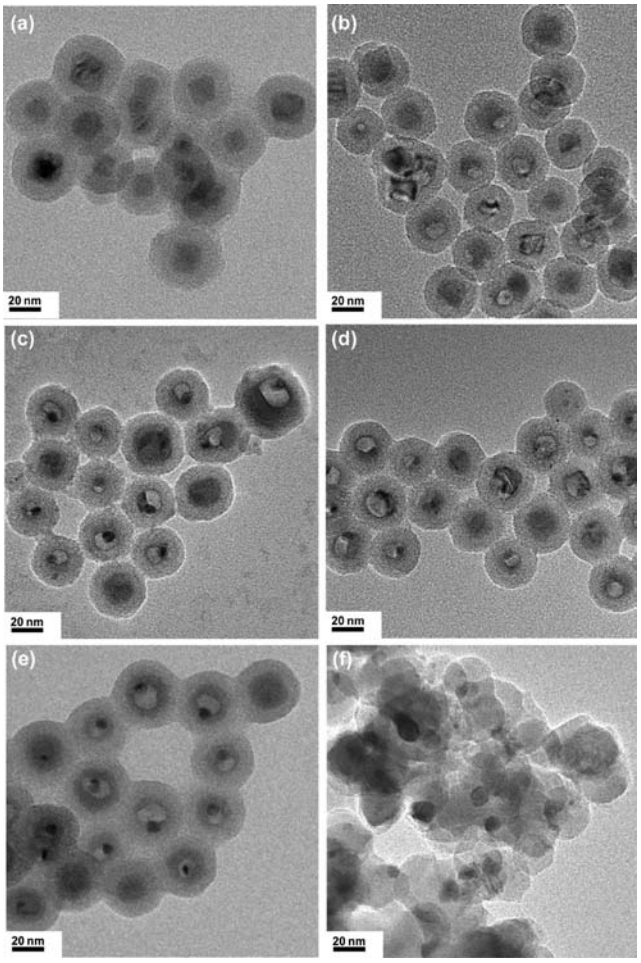

Figure 12. TEM images of the $MnO/Ni^{2+}@SiO_2$ nanospheres (a) before and after the annealing under the reductive environment at 500 °C for (b) 0 h, (c) 2 h, and (d) 5 h, (e) at 600 °C for 2 h, and (f) at 700 °C for 5 h.

interface between the MnO core and the SiO_2 shell of the $MnO@SiO_2/Ni(II)$ nanospheres provided a preferential site for the nucleation and growth of a single Ni nanocrystal (Figure 13).[13] When silica nanospheres containing Ni^{2+} complexes were prepared in the absence of MnO nanoparticles and treated at high temperature, for the control purpose, it generated multiple numbers of tiny Ni nanocrystals distributed over the silica spheres (Figure S4). The oxidative annealing of Ni@HSNP-500 gave rise to the growth of an $NiMn_2O_4$ phase inside the cavity, thus resulting in the formation of $NiMn_2O_4@SiO_2$ nanospheres consisting of a crystalline $NiMn_2O_4$ core and amorphous silica shells (Figure 14).

When the $NiMn_2O_4@SiO_2$ nanospheres were reductively annealed under conditions suitable for examining possible

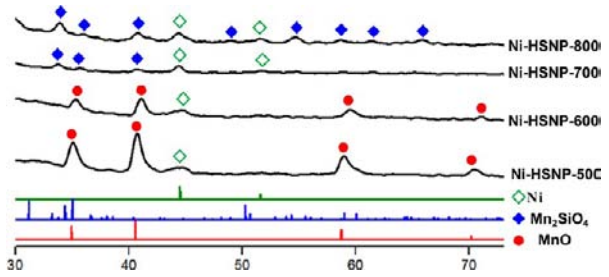

Figure 13. XRD patterns of the $MnO/Ni^{2+}@SiO_2$ nanosphere before and after the annealing at various conditions.

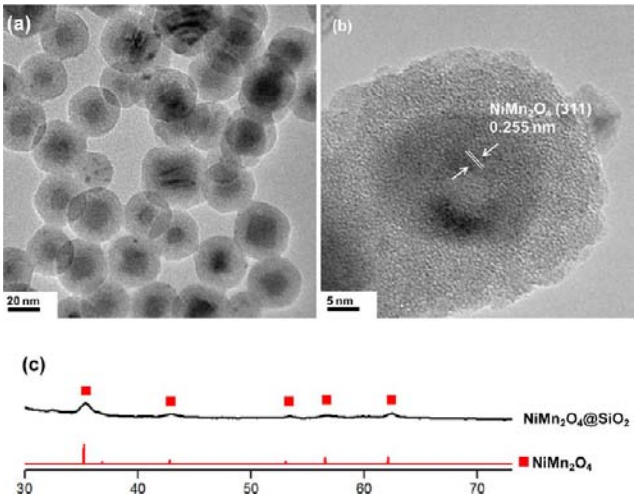

Figure 14. (a) TEM and (b) HRTEM images and (c) XRD pattern of the $NiMn_2O_4@SiO_2$.

transformation to a hollow structure, the $NiMn_2O_4$ core was not reduced and did not react with silica under the annealing conditions. Therefore, any further changes were not detected in the morphology and crystalline phase of the $NiMn_2O_4@SiO_2$.

4. CONCLUSION

In summary, in the course of a study of confined reactions of MnO nanocrystals inside silica nanospheres, we found transformation to a hollow structure as a result of outward diffusion of MnO species into the thermodynamically more stable silicate phase of the shell. It was also discovered that oxidation reconverts the hollow nanostructure to the solid-core structure through the growth of SiO_2-immiscible Mn_3O_4 grains inside the cavities. By introducing the catalytic Pt nanocrystals, which enable the low-temperature reduction of Mn_3O_4, we successfully demonstrated a reversible transformation from solid to hollow and again to a hollow nanostructure, which can be cycled as a function of the gas environment. This result suggests that the reversible and controllable conversion between hollow and solid nanostructure with contrasting properties can be achieved by designing the core−shell system in which the phase-miscibility between core and shell materials can be intentionally switched. We believe that this reversible and cyclical transformation between solid and hollow structures could be used to develop environment-responsive systems with switchable performances. Future research efforts will be directed toward this end.

dx.doi.org/10.1021/ja309142j | J. Am. Chem. Soc. 2013, 135, 1378−1385

■ ASSOCIATED CONTENT

Supporting Information

Additional TEM images and XRD patterns. This material is available free of charge via the Internet at http://pubs.acs.org.

■ AUTHOR INFORMATION

Corresponding Author

insulee97@postech.ac.kr

Author Contributions

§T.-L.H. and J.G.K. contributed equally to this work.

Notes

The authors declare no competing financial interest.

■ ACKNOWLEDGMENTS

This work was supported by the National Research Foundation of Korea (NRF) grant funded by the Korea government (MEST) (2011-0017377).

■ REFERENCES

(1) (a) Cushing, B. L.; Kolesnichenko, V. L.; O'Connor, C. J. *Chem. Rev.* **2004**, *104*, 3893−3946. (b) Roucoux, A.; Schulz, J.; Patin, H. *Chem. Rev.* **2002**, *102*, 3757−3778.

(2) For general reviews on nanocrystal conversion chemistry, see: (a) Moon, G. D.; Ko, S.; Min, Y.; Zeng, J.; Xia, Y.; Jeong, U. *Nano Today* **2011**, *6*, 186−203. (b) Vasquez, Y.; Henkes, A. E.; Bauer, J. C.; Schaak, R. E. *J. Solid State Chem.* **2008**, *181*, 1509−1523.

(3) (a) Moon, G. D.; Ko, S.; Xia, Y.; Jeong, U. *ACS Nano* **2010**, *4*, 2307−2319. (b) Leonard, B. M.; Anderson, M. E.; Oyler, K. D.; Phan, T.-H.; Schaak, R. E. *ACS Nano* **2009**, *3*, 940−948. (c) Muthuswamy, E.; Kharel, P. R.; Lawes, G.; Brock, S. L. *ACS Nano* **2009**, *3*, 2383−2393. (d) Luther, J. M.; Zheng, H.; Sadtler, B.; Alivisatos, A. P. *J. Am. Chem. Soc.* **2009**, *131*, 16851−16857.

(4) For recent reviews on hollow nanoparticles, see: (a) Hu, J.; Chen, M.; Fang, X.; Wu, L. *Chem. Soc. Rev.* **2011**, *40*, 5472−5491. (b) Liu, J.; Qiao, S. Z.; Chen, J. S.; Lou, X. W.; Xing, X.; Lu, G. Q. *Chem. Commun.* **2011**, *47*, 12578−12591. (c) Zhang, Q.; Wang, W.; Goebl, J.; Yin, Y. *Nano Today* **2009**, *4*, 494−507. (d) Lou, X. W.; Archer, L. A.; Yang, Z. *Adv. Mater.* **2008**, *20*, 3987−4019.

(5) (a) Lee, I.; Joo, J. B.; Yin, Y.; Zaera, F. *Angew. Chem., Int. Ed.* **2011**, *50*, 10208−10211. (b) Sanlés-Sobrido, M.; Pérez-Lorenzo, M.; Rodríguez-González, B.; Salgueiriño, V.; Correa-Duarte, M. A. *Angew. Chem., Int. Ed.* **2012**, *51*, 3877−3882. (c) Fang, X.; Liu, Z.; Hsieh, M.-F.; Chen, M.; Liu, P.; Chen, C.; Zheng, N. *ACS Nano* **2012**, *6*, 4434−4444. (d) Yeo, K. M.; Choi, S.; Anisur, R. M.; Kim, J.; Lee, I. S. *Angew. Chem., Int. Ed.* **2011**, *50*, 745−748.

(6) (a) An, K.; Hyeon, T. *Nano Today* **2009**, *4*, 359−373. (b) Tang, S.; Huang, X.; Chen, X.; Zheng, N. *Adv. Funct. Mater.* **2010**, *20*, 2442−2447. (c) Liu, J.; Qiao, S. Z.; Hartono, S. B.; Lu, G. Q. *Angew. Chem., Int. Ed.* **2010**, *49*, 4981−4985. (d) Cheng, K.; Peng, S.; Xu, C.; Sun, S. *J. Am. Chem. Soc.* **2009**, *131*, 10637−10644.

(7) (a) Kim, T.; Momin, E.; Choi, J.; Yuan, K.; Zaidi, H.; Kim, J.; Park, M.; Lee, N.; McMahon, M. T.; Quinones-Hinojosa, A.; Bulte, J. W. M.; Hyeon, T.; Gilad, A. A. *J. Am. Chem. Soc.* **2011**, *133*, 2955−2961. (b) Chen, Y.; Chen, H.; Zeng, D.; Tian, Y.; Chen, F.; Feng, J.; Shi, J. *ACS Nano* **2010**, *4*, 6001−6013. (c) Shin, J.; Anisur, R. M.; Ko, M. K.; Im, G. H.; Lee, J. H.; Lee, I. S. *Angew. Chem., Int. Ed.* **2009**, *48*, 321−324.

(8) (a) Wang, Z.; Zhou, L.; Lou, X. W. *Adv. Mater.* **2012**, *24*, 1903−1911. (b) Koo, B.; Xiong, H.; Slater, M. D.; Prakapenka, V. B.; Balasubramanian, M.; Podsiadlo, P.; Johnson, C. S.; Rajh, T.; Shevchenko, E. V. *Nano Lett.* **2012**, *12*, 2429−2435. (c) Ding, S.; Chen, J. S.; Qi, G.; Duan, X.; Wang, Z.; Giannelis, E. P.; Archer, L. A.; Lou, X. W. *J. Am. Chem. Soc.* **2011**, *133*, 21−23.

(9) (a) Yin, Y.; Erdonmez, C.; Aloni, S.; Alivisatos, A. P. *J. Am. Chem. Soc.* **2006**, *128*, 12671−12673. (b) Sun, Y.; Mayers, B.; Xia, Y. *Adv. Mater.* **2003**, *15*, 641−646. (c) Sun, Y.; Xia, Y. *Science* **2002**, *298*, 2176−2179.

(10) (a) Henkes, A. E.; Vasquez, Y.; Schaak, R. E. *J. Am. Chem. Soc.* **2007**, *129*, 1896−1897. (b) Peng, S.; Sun, S. *Angew. Chem., Int. Ed.* **2007**, *46*, 4155−4158. (c) Gao, J.; Zhang, B.; Zhang, X.; Xu, B. *Angew. Chem., Int. Ed.* **2006**, *45*, 1220−1223. (d) Yin, Y.; Rioux, R. M.; Erdonmez, C. K.; Hughes, S.; Somorjai, G. A.; Alivisatos, A. P. *Science* **2004**, *304*, 711−714.

(11) (a) Xiong, S.; Zeng, H. C. *Angew. Chem., Int. Ed.* **2012**, *51*, 949−952. (b) Park, J.; Zheng, H.; Jun, Y.; Alivisatos, A. P. *J. Am. Chem. Soc.* **2009**, *131*, 13943−13945.

(12) Examples on the reversible morphology change of the nanoparticles: (a) Dinda, E.; Biswas, M.; Mandal, T. K. *J. Phys. Chem. C* **2011**, *115*, 18518−18530. (b) Karan, N. S.; Sarkar, S.; Sarma, D. D.; Kundu, P.; Ravishankar, N.; Pradhan, N. *J. Am. Chem. Soc.* **2011**, *133*, 1666−1669. (c) Cabié, M.; Giorgio, S.; Henry, C. R.; Axet, M. R.; Philippot, K.; Chaudret, B. *J. Phys. Chem. C* **2010**, *114*, 2160−2163. (d) Nolte, P.; Stierle, A.; Jin-Phillipp, N. Y.; Kasper, N.; Schulli, T. U.; Dosch, H. *Science* **2008**, *321*, 1654−1658.

(13) Examples on the interconversion between hollow and solid nanostructures: (a) Chenna, S.; Crozier, P. A. *Micron* **2012**, *43*, 1188. (b) Chenna, S.; Banerjee, R.; Crozier, P. A. *ChemCatChem* **2011**, *3*, 1051−1059. (c) Nakamura, R.; Tokozakura, D.; Lee, J.-G.; Mori, H.; Nakajima, H. *Acta Mater.* **2008**, *56*, 5276−5284. (d) Nakamura, R.; Lee, J.-G.; Mori, H.; Nakajima, H. *Philos. Mag.* **2008**, *88*, 257−264.

(14) (a) Shin, J.; Ha, T.-L.; Lee, I. S. *Eur. J. Inorg. Chem.* **2010**, 357−360. (b) Shin, J.; Kim, H.; Lee, I. S. *Chem. Commun.* **2008**, 5553−5555.

(15) Na, H. N.; Lee, J. H.; An, K.; Park, Y. I.; Park, M.; Lee, I. S.; Nam, D.-H.; Kim, S. T.; Kim, S.-H.; Kim, S.-W.; Lim, K.-H.; Kim, K.-S.; Kim, S.-O.; Hyeon, T. *Angew. Chem., Int. Ed.* **2007**, *46*, 5397−5401.

(16) (a) Anisur, R. M.; Shin, J.; Choi, H. H.; Yeo, K. M.; Kang, E. J.; Lee, I. S. *J. Mater. Chem.* **2010**, *20*, 10615−10621. (b) Lee, D. C.; Mikulec, F. V.; Pelaez, J. M.; Koo, B.; Korgel, B. A. *J. Phys. Chem. B* **2006**, *110*, 11160−11166. (c) Yi, D. K.; Selvan, S. T.; Lee, S. S.; Papaefthymiou, G. C.; Kundaliya, D.; Ying, J. Y. *J. Am. Chem. Soc.* **2005**, *127*, 4990−4991.

(17) (a) Sun, H.; Qin, X.; Zaera, F. *J. Phys. Chem. Lett.* **2011**, *2*, 2525−2530. (b) Ablett, J. M.; Woicik, J. C.; Tőkei, Z.; List, S.; Dimasi, E. *Appl. Phys. Lett.* **2009**, *94*, 042112/1−042112/3. (c) Koike, J.; Haneda, M.; Iijima, J.; Otsuka, Y.; Sako, H.; Neishi, K. *J. Appl. Phys.* **2007**, *102*, 043527/1−043527/7.

(18) (a) Zaitsev, A. I.; Mogutnov, B. M. *Inorg. Mater.* **1997**, *33*, 823−831. (b) Eriksson, G.; Wu, P.; Blander, M.; Pelton, A. D. *Can. Metall. Q.* **1994**, *33*, 13−21. (c) Rao, B. K. D. P.; Gaskell, D. R. *Metall. Trans. B* **1981**, *12B*, 311−317.

(19) (a) Yang, Y.; Yang, R. B.; Fan, H. J.; Scholz, R.; Huang, Z.; Berger, A.; Qin, Y.; Knez, M.; Gösele, U. *Angew. Chem., Int. Ed.* **2010**, *49*, 1442−1446. (b) Zhou, J.; Liu, J.; Wang, X.; Song, J.; Tummala, R.; Xu, N. S.; Wang, Z. L. *Small* **2007**, *3*, 622−626. (c) Fan, H. J.; Knez, M.; Scholz, R.; Nielsch, K.; Pippel, E.; Hesse, D.; Zacharias, M.; Gösele, U. *Nat. Mater.* **2006**, *5*, 627−631.

(20) Reed, C.; Lee, Y.-K.; Oyama, S. T. *J. Phys. Chem. B* **2006**, *110*, 4207−4216.

(21) (a) Zafar, Q.; Mattisson, T.; Gevert, B. *Ind. Eng. Chem. Res.* **2005**, *44*, 3485−3496. (b) Zafar, Q.; Mattisson, T.; Gevert, B. *Energy Fuels* **2006**, *20*, 34−44.

(22) Töpfer, J.; Diekmann, R. *Solid State Ionics* **2010**, *181*, 479−488.

(23) (a) Feio, L. S. F.; Hori, C. E.; Damyanova, S.; Noronha, F. B.; Cassinelli, W. H.; Marques, C. M. P.; Bueno, J. M. C. *Appl. Catal., A* **2007**, *316*, 107−116. (b) Baylet, A.; Royer, S.; Labrugère, C.; Valencia, H.; Marécot, P.; Tatibouët, J. M.; Duprez, D. *Phys. Chem. Chem. Phys.* **2008**, *10*, 5983−5992.

(24) (a) Jozwiak, W. K.; Kaczmarek, E.; Maniecki, T. P.; Ignaczak, W.; Maniukiewicz, W. *Appl. Catal., A* **2007**, *326*, 17−27. (b) Matsuda, T.; Hanai, A.; Uchijima, F.; Sakagami, H.; Takahashi, N. *Microporous Mesoporous Mater.* **2002**, *51*, 155−164.